Estimating the Performance of Patched Multirevolution Solar-Sail Transfers Around Planets

Gámez Losada, F.; Visser, P.N.A.M.; Heiligers, M.J.

DOI
10.2514/1.G009233

Publication date
2026

Document Version
Final published version

Published in
Journal of Guidance, Control, and Dynamics: devoted to the technology of dynamics and control

Journal of Guidance, Control, and Dynamics
Vol. 49, No. 1, January 2026

Estimating the Performance of Patched Multirevolution Solar-Sail Transfers Around Planets

Fernando Gámez Losada,* Pieter Visser,† and Jeannette Heiligers‡
Delft University of Technology, 2628 CD Delft, The Netherlands

https://doi.org/10.2514/1.G009233

Understanding of what is achievable with solar-sail technology around planetary bodies is in its infancy. The seemingly simple problem of transferring from one circular orbit to another circular orbit with a solar sail around a planet is yet to be fully characterized. This work aims to start filling that gap by analyzing the coplanar patched multirevolution circular-to-circular (PMC2C) transfer. The PMC2C transfer is a continuous sequence of single-revolution circular-to-circular (SC2C) transfers, where each SC2C transfer is optimized for the achieved radius change in one orbital revolution. Then, the radius change and transfer time of a PMC2C transfer is obtained as the aggregation of the individual SC2C increments. To generalize to all initial geometries, hundreds of PMC2C transfers must be computed, which is not feasible in practice. To bypass this problem, the so-called patched method is proposed. The patched method uses a semianalytical approach to estimate the radius change and the transfer time of the PMC2C transfers, effectively removing the need for numerical optimization. Dimensionless in nature, the patched method can be used for any sail design around any planet orbiting a star. With this tool, early mission design is greatly simplified; hundreds of trajectories can be analyzed in a matter of minutes. In addition, the generalized formulation reveals the best and worst orbital geometries and initial epochs to start a PMC2C transfer, improving general knowledge of how to "sail" around planets.

I. Introduction

ALTHOUGH the bulk of solar-sail astrodynamics research is focused on heliocentric trajectories, most missions (except Interplanetary Kite-craft Accelerated by Radiation Of the Sun [1]) have flown around Earth [2–5]. The newly launched Advanced Composite Solar Sail System mission is the most recent example [6]. However, a proper understanding of how to sail around planets is still in its infancy, possibly due to the great challenges posed by planet-bound sailing [7].

Previous research on planet-centered solar sailing focused on escape trajectories or open-ended trajectories (e.g., pure orbit raising or inclination-change maneuvers) [8–14]. The few works that did consider orbit transfers did not approach the problem in a generalized fashion, mostly providing insights into specific examples. For example, in [15], Fitzgerald used pseudospectral optimal control mixed with averaging techniques to characterize a transfer from geosynchronous transfer orbit (GTO) to geosynchronous equatorial orbit (GEO) for various sail performances. Two different transfer regimes were observed, where the bifurcation point was reached when the transfer time surpassed one year. Although the paper demonstrated that solar sails can tackle complex three-dimensional planet-centered transfers, only the particular case of one GTO-to-GEO transfer was analyzed. In [16], Kelly and Bevilacqua proposed a solar-sail mission to remove debris from GEO. A complete dynamical model that included eclipsing was defined for the simulations, proving the viability of the proposed concept. Nonetheless, again, only specific transfers around the GEO region were considered. In [17], Bianchi et al. brought the solar-sail debris removal concept to low Earth orbit (LEO). A preliminary mission divided into multiple phases was showcased, where the various transfers involved were computed using blending of locally optimal control laws. Again, only one particular case study was contemplated in the analyses; the influence of different geometries and initial epochs was not investigated in detail. The work in [18] came closest to a generalization of the planet-centered transfer problem, where Oguri et al. provided a means to achieve any desired planet-centered transfer in a locally optimal manner through the solar-sailing Q-law, effectively solving the transfer problem for medium Earth orbit (MEO) and beyond. Several examples were provided to showcase the performance of the solar-sailing Q-law. However, the inherent physics of the transfer problem were not entirely exposed. A clear understanding of the general transfer capabilities of solar sails is therefore still lacking.

In our latest work [19], we analyzed the simplest conceivable planet-centered transfer: the coplanar single-revolution circular-to-circular (SC2C) orbit transfer. The objective of the SC2C transfer is defined as maximizing the orbital radius within one orbital revolution, starting from, and ending, in planar circular patched multirevolution circular-to-circular (PMC2C) orbits. Our goal in the current paper is to extrapolate the results presented in [19] for the SC2C transfer to the multirevolution case. We construct lengthy multirevolution trajectories by patching together a series of sequentially optimized SC2C transfers and refer to these new trajectories as coplanar PMC2C orbit transfers. In theory, a solar sail can transfer between any two coplanar circular orbits by means of such a PMC2C transfer. Although not optimal, the PMC2C transfers are valid transfers that can be used as initial guesses to initialize an optimal control solver (which is left for future work).

A generalized understanding of the PMC2C transfers requires us to consider a wide range of sail designs, orbital geometries, and mission scenarios, for which thousands of PMC2C transfers would have to be computed. Due to the low thrust provided by near-term solar-sail technology, a modest PMC2C transfer of a few hundred kilometers already entails hundreds of SC2C transfers, making the computational load too demanding. To circumvent this issue, we developed the so-called "patched method". The patched method uses a semianalytical formulation and the characteristics of the SC2C transfer to provide quick estimates of the transfer time and radius change (i.e., the performance) of the PMC2C transfers. Furthermore, the method is dimensionless, which makes it valid around any planet and for any given orbit geometry, initial time, and solar-sail performance. We use the power of the patched method to

Presented as Paper 25-221 at the 2025 AAS/AIAA Space Flight Mechanics Meeting, Kaua'i, Hawaii, 19–23 January, 2025; received 1 April 2025; accepted for publication 16 July 2025; published online Open Access 14 October 2025.

*Ph.D. Candidate, Astrodynamics and Space Missions; F.GamezLosada@tudelft.nl (Corresponding Author).

†Full Professor, Astrodynamics and Space Missions; P.N.A.M.Visser@tudelft.nl.

‡Associate Professor, Astrodynamics and Space Missions; M.J.Heiligers@tudelft.nl.

show how the transfer performance varies with orbit geometry and initial time, unveiling previously unknown characteristics that are particular to solar-sail transfers.

The remainder of the article is organized as follows. Section II describes the dynamical framework used in the study. Section III summarizes our previous work on SC2C transfers, as the results are needed in the formulation of the patched method. Section IV extrapolates the SC2C transfer to the many-revolution case through the PMC2C transfer. Section V elaborates on the patched method, and Sec. VI validates the predictions of the patched method against a set of numerically computed PMC2C transfers. Finally, Sec. VII gathers the conclusions that can be drawn from this work.

II. Dynamics

To define the transfer problem, we make use of two inertial reference frames centered at the planet: the ecliptic reference frame $E(x_e, y_e, z_e)$, and the orbital reference frame $I(x, y, z)$. Figure 1 gathers schematics of both frames.

Figure 1a shows the ecliptic reference frame $E(x_e, y_e, z_e)$ and the orbital plane. The ecliptic reference frame is centered at the planet, with the x_e axis aligned with the sun–planet direction $\widehat{\boldsymbol{S}}$ at the initial epoch (e.g., for Earth, at the autumnal equinox). The z_e axis is aligned with the ecliptic north pole, and the y_e axis completes the right-handed triad. The orientation of the orbital plane is given by the inclination i and the right ascension of the ascending node (RAAN) Ω in the ecliptic frame. While the orbital plane remains fixed in inertial space, the sun–planet direction $\widehat{\boldsymbol{S}}$ rotates counterclockwise in the ecliptic plane with a period P equal to the planet's orbital period. Note that, for the remainder of the paper, we refer to one orbital period of the planet around the sun as a year.

Figure 1b shows the orbital reference frame $I(x, y, z)$, which is also centered at the planet: the x axis matches the line of nodes, the z axis is parallel to the orbit's angular momentum vector $\boldsymbol{h}$, and the y axis completes the right-handed triad. The orbital reference frame is used to formulate the equations of motion (EOMs).

Of importance to this work is the aspect angle β, defined as the angle between the sun–planet direction $\widehat{\boldsymbol{S}}$ and the angular momentum vector $\boldsymbol{h}$ (see Fig. 1b). The aspect angle determines the illumination conditions of the orbital plane: for $\beta = 0$ deg and $\beta = 90$ deg, the orbit is perpendicular and parallel to the incoming sunlight, respectively. The aspect angle changes periodically due to the yearly motion of $\widehat{\boldsymbol{S}}$ (see Sec. IV.B). Finally, note that the sun is assumed to be infinitely far away from the planet (i.e., all sun rays are parallel to $\hat{\boldsymbol{S}}$).

In this work, we adopt a simplified dynamical model: the motion of the solar sail around the planet is described by accounting only for point-mass gravity and the solar-sail acceleration, which is modeled by assuming an ideal solar sail [7]. Then, in the orbital frame, the EOMs adopt the form

$$\frac{\mathrm{d}\boldsymbol{r}}{\mathrm{d}t} = \boldsymbol{v}, \quad \frac{\mathrm{d}\boldsymbol{v}}{\mathrm{d}t} = -\frac{\mu}{r^3}\boldsymbol{r} + a_0\left(\widehat{\boldsymbol{S}}\cdot\widehat{\boldsymbol{n}}\right)^2\widehat{\boldsymbol{n}} \tag{1}$$

where $\boldsymbol{r}$ is the position vector, $\boldsymbol{v}$ the velocity vector, t the independent variable time, μ the planet's gravitational constant, a_0 the solar-sail characteristic acceleration at the planet's average distance from the sun, and $\widehat{\boldsymbol{n}}$ the normal vector perpendicular to the solar-sail surface. Note that eclipses are not considered in Eq. (1). Numerical integration of Eq. (1) with the initial state $(\boldsymbol{r}_0, \boldsymbol{v}_0)$ at $t = 0$ and the control law $\widehat{\boldsymbol{n}} = \widehat{\boldsymbol{n}}(t)$ provides the trajectory of the solar sail $(\boldsymbol{r} = \boldsymbol{r}(t), \boldsymbol{v} = \boldsymbol{v}(t))$ around the planet.

The trajectory of the solar sail is assumed to be two-dimensional and contained in the orbital plane. This assumption is enforced by neglecting the out-of-plane component of the solar-sail acceleration [i.e., $a_0(\widehat{\boldsymbol{S}}\cdot\widehat{\boldsymbol{n}})^2\widehat{\boldsymbol{n}}\cdot\hat{\boldsymbol{z}}$] in the EOMs; only the in-plane solar-sail acceleration is considered in the EOMs. Note that, because the magnitude of the solar-sail acceleration is only small and the control is periodic [19], the out-of-plane motion during the transfer will be equally small.

To improve stability during the numerical optimization, the EOMs are scaled using the initial position, velocity, and orbital period $T_0 = 2\pi\sqrt{r_0^3/\mu}$, yielding

$$\frac{\mathrm{d}\boldsymbol{\rho}}{\mathrm{d}\tau} = 2\pi\boldsymbol{\xi}, \quad \frac{\mathrm{d}\boldsymbol{\xi}}{\mathrm{d}\tau} = 2\pi\left[-\frac{\boldsymbol{\rho}}{\rho^3} + \Psi\boldsymbol{u}\right] \tag{2}$$

where $\boldsymbol{\rho} = \boldsymbol{r}/r_0$, $\boldsymbol{\xi} = \boldsymbol{v}/v_0$, $\tau = t/T_0$, $\boldsymbol{u} = (\widehat{\boldsymbol{S}}\cdot\widehat{\boldsymbol{n}})^2\widehat{\boldsymbol{n}}$, and $\Psi = a_0/g_0$. Note that $g_0 = \mu/r_0^2$ is the local gravitational acceleration at the initial state.

The scaled EOMs in Eq. (2) only depend on one dimensionless parameter, which is the scaled characteristic acceleration Ψ, which represents the "strength" of the sail relative to the local gravity. A particular sail design orbiting a planet will yield a smaller Ψ the closer it gets to the planet. Note that, because the problem is scaled, two real problems (e.g., initial circular orbits around Mars and Earth) with the same scaled initial conditions, control $\boldsymbol{u} = \boldsymbol{u}(\tau)$ and Ψ yield the same scaled trajectory. As shown throughout the paper, the scaled formulation allows for easy computation of transfer performances for any sail performance, which is a great characteristic for preliminary solar-sail sizing studies.

III. Single-Revolution Transfers

In this section, we summarize the main results and conclusions of our previous work. In [19], we characterized the simplest form of planet-centered solar-sail transfer: the SC2C transfer. Here, we condense the main results, as they will be needed for the formulation of the patched method in Sec. V. In particular, we show the performance of the SC2C transfer, which constitutes the building block of

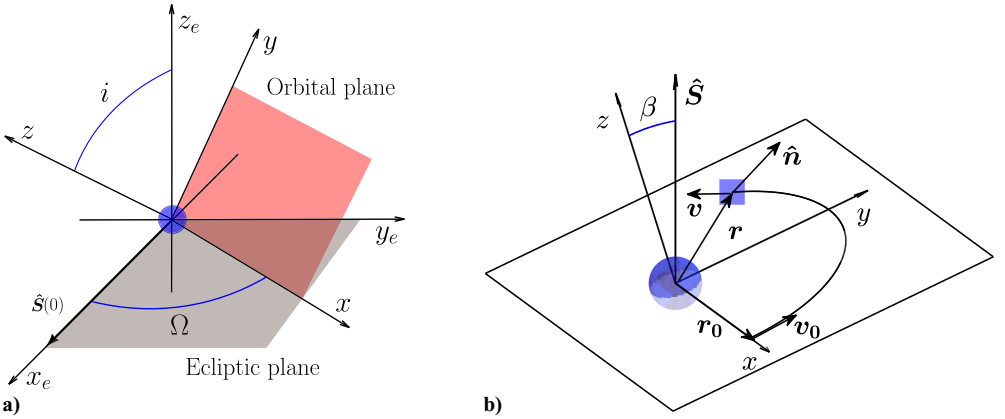

Fig. 1 Schematics of a) ecliptic reference frame $E(x_e, y_e, z_e)$, and orientation of the orbital plane; and b) orbital reference frame $I(x, y, z)$, together with the relevant variables involved in the formulation of the equations of motion.

the transfers presented in Sec. IV. In this context, performance is understood as achieved radius change after one orbital revolution.

A. Optimization Problem

The SC2C transfers arise as the solution to the following optimization problem:

$$\max_{\boldsymbol{u}\in\mathcal{B}}\{r(t_f)\} \quad \text{s.t. EOMs \& } e(t_f) = 0 \tag{3}$$

where $\boldsymbol{u}$ is the control vector, $\mathcal{B}$ the set of admissible controls, r the orbital radius, EOMs the equations of motion with associated initial conditions (see Sec. II), e the osculating eccentricity, and t_f the final time. The SC2C transfer is defined to span one orbital revolution, meaning that, at t_f, the initial and final position vectors are parallel. Due to the small magnitude of the solar-sail acceleration, the radius change will be small, and the final time will thus be approximately equal to the initial orbital period. Note that, when computing SC2C transfers, we neglect the motion of the sun as viewed from the planet (i.e., $\widehat{\boldsymbol{S}}$ is constant) because the transfer time is significantly shorter than the orbital period of the sun around the planet.

To solve the optimization problem posed in Eq. (3), we used the commercially available General Purpose OPtimal Control Software II software [20]. GPOPS-II uses direct collocation (i.e., variable-order Gaussian quadrature methods) to translate the continuous optimal control problem into a nonlinear program that is then solved with Interior Point OPTimizer [21]. The automatic differentiation toolbox ADiGator is used to obtain the required first- and second-order derivatives of the dynamics, cost function, and constraints [22].

B. Performance

The performance of the SC2C transfer is defined as the achieved radius change scaled with the initial radius:

$$\eta = \frac{\delta r}{r_0} \tag{4}$$

where δr is the change in orbital radius obtained from solving Eq. (3).

In our previous work [19], it was found that the performance depends on two parameters: the aspect angle β and the scaled characteristic acceleration Ψ. Moreover, we concluded that these dependencies could be separated as a product of two different functions [19]:

$$\eta = \eta_r(\Psi)\,\chi(\beta) \tag{5}$$

where the reference performance function η_r only depends on Ψ, and the mapping function χ only depends on β. The reference performance function is computed by repeatedly solving Eq. (3) for different values of Ψ while keeping the aspect angle constant and equal to $\beta = 40$ deg. Hence, η_r indicates how the performance changes with altitude or sail design at an aspect angle of $\beta = 40$ deg. The mapping function χ is obtained by following the same procedure but varying β and keeping Ψ constant. Then, χ shows how the performance varies with the aspect angle and can be used to "map" η_r to aspect angles different from $\beta = 40$ deg. Using both functions, we can effectively compute the performance of any possible SC2C transfer.

Figure 2 gathers the plots of the mapping and reference performance functions. The main observations can be summarized as follows:

1) From Fig. 2a, it is clear that the performance drops significantly as the aspect angle increases, where the best performance is achieved for $\beta = 0$ deg (i.e., the incoming sunlight is perpendicular to the orbital plane), and the minimum performance is achieved for $\beta = 90$ deg (i.e., the incoming sunlight is parallel to the orbital plane).

2) From Fig. 2b, we can see that the reference performance function is linear in Ψ in log–log scale and increases for increasing values of Ψ. Recall that Ψ is defined as the ratio of the characteristic acceleration over the local gravitational acceleration. Hence, for a fixed sail design (i.e., constant a_0), the performance increases with altitude. Or, equivalently, for a fixed altitude, performance increases with a_0.

3) The linearity in log–log scale shown in Fig. 2b breaks down at large values of the scaled characteristic acceleration. At sufficiently large values of Ψ, the solar sail is "blown away" from the planetary system before it completes the SC2C transfer because the gravity of the planet is too small to balance the solar-sail acceleration. It is found that for $\Psi < 1 \times 10^{-2}$, Eq. (5) and Fig. 2 remain valid.

To compute the plots in Fig. 2, one could choose a value for β different than 40 deg. For example, if $\beta = 20$ deg is used, χ will be equal to one at 20 deg rather than at 40 deg (see Fig. 2a), and the line representing η_r in Fig. 2b will shift downward but remain parallel to the one shown in the plot (i.e., different vertical axis intercept, same slope). In other words, the choice for β in the computation of Fig. 2 is arbitrary and does not have an impact on the results. Similarly, because χ does not depend on Ψ, one can compute Fig. 2a for any arbitrary value of Ψ and always obtain the same curve (consult [19] for a detailed proof).

The main limitation of the plots in Fig. 2 is that eclipses are not considered. When the sail enters the eclipse region, it cannot generate thrust. The effect on the performance of the SC2C transfers is yet to be analyzed, but it surely will entail a performance loss. However, independently from the orbit altitude, the smaller the aspect angle, the smaller the chances of entering eclipse, where at the limit of $\beta = 0$ deg, eclipses never occur; eclipses will therefore mostly affect the performance at large aspect angles, where the performance is already low (see Fig. 2a). Hence, we foresee that the effects of eclipsing events will not have a profound impact on the general conclusions drawn from Fig. 2.

Another limitation of the plots in Fig. 2 comes from the assumption of an ideal solar-sail model. The ideal model considers the membrane of the sail to be flat and perfectly reflective (i.e., a spotless mirror). In reality, the membrane emits, absorbs, and

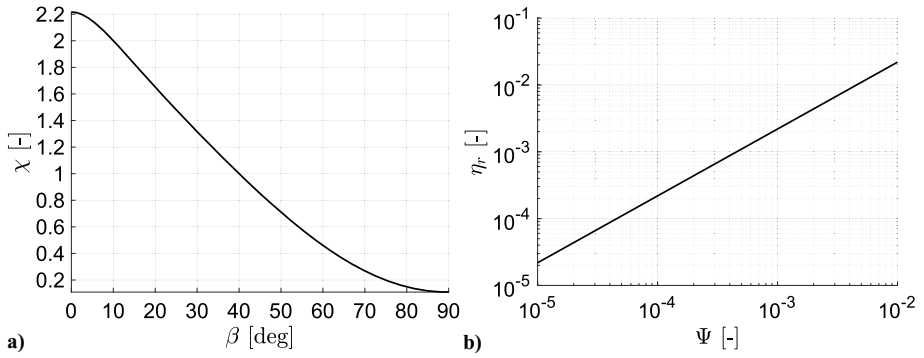

Fig. 2 Functions that define the performance of the single-revolution circular-to-circular transfer: a) mapping function, and b) reference performance function.

reflects radiation. In addition, the membrane of the sail contains wrinkles and billows under the solar radiation pressure once in orbit, implying that, in reality, the membrane is not perfectly flat. Both wrinkles and billowing cause a performance loss, but the trends observed in Fig. 2 should remain unaltered. Of more importance is the effect of the nonideal optical properties of the sail. The more refined optical solar-sail model shows that, for increasing values of the cone angle (i.e., the angle between the sun–planet line and the sail's normal vector), the thrust vector is no longer aligned with the sail's normal vector (i.e., the tangential component becomes dominant) [7]. In [19], it was shown that, as the aspect angle increases, the domain of the cone angle needed to execute the SC2C transfer also increases, where at the limit $\beta = 90$ deg, the domain of the cone angle is as high as (65, 90) deg. For such high cone angles, the solar-sail acceleration obtained with a high-fidelity model deviates significantly from that obtained with the ideal model. Hence, it is expected that if a high-fidelity model is used, the curve in Fig. 2a will change, with the differences increasing for increasing aspect angles. Nevertheless, it is reasonable to assume that the main conclusions drawn from Fig. 2 will still hold. We chose the ideal model to provide a generalized set of closed-form equations that allowed us to derive previously unknown characteristics of the planet-centered solar-sail transfer problem. Higher-fidelity solar-sail models are usually tailored to a specific sail design and are not suitable for generalization.

For use in the computation of the performance of the PMC2C transfers, an analytical expression for the mapping function is needed, which is obtained by fitting an eighth degree polynomial to the data in Fig. 2a. The polynomial is expressed as $\chi = \sum_{j=0}^{8} p_j \beta^j$ for $\beta \in [0, \pi/2]$, where the coefficients are: $p_0 = = 2.21529426884005$, $p_1 = 0.083872533726236$, $p_2 = -12.4503541592147$, $p_3 = 37.8806339189659$, $p_4 = -65.4280684988028$, $p_5 = 67.6438452545547$, $p_6 = -41.163077357\,5200$, $p_7 = 13.6413368229864$, and $p_8 = -1.90025732895530$. Note that the mapping function $\chi(\beta)$ is symmetric with respect to $\beta = 90$ deg [e.g., $\chi(60) = \chi(120)$] but that, for conciseness, Fig. 2a only shows the left half of the mapping function. Similarly, the reference performance function is fitted to a power law of the form $\eta_r = n\Psi^m$, where the resulting coefficients are $n = 2.19795377389429$ and $m = 1.00062884835663$.

IV. Multirevolution Transfers

In this section, we extrapolate the results presented in Sec. III for the SC2C transfer to the multirevolution case. To put it simply, we construct lengthy multirevolution trajectories by patching together a series of sequential SC2C transfers. We refer to these new trajectories as PMC2C transfers. Because of the circularization that occurs at each orbital revolution, the PMC2C transfer is not globally optimal, but the result is a valid solar-sail transfer trajectory between two arbitrarily separated circular orbits. As such, it can be used as an initial guess for a more refined multirevolution trajectory optimization process. Future work will look into using the PMC2C transfers for that purpose.

Figure 3 depicts a schematic of the patching procedure, where the individual SC2C transfers are shown in different colors. Each SC2C transfer is optimized sequentially: the final conditions of the current SC2C transfer become the initial conditions of the next SC2C transfer. The process of generating a PMC2C transfer is computationally intense. Hundreds of SC2C transfers have to be optimized to assemble a single PMC2C transfer. Nevertheless, the process is robust and straightforward. The only limitations occur at high altitudes, where the gravity of the planet becomes too low and the sailcraft flies away from the planetary system, or the aspect angle changes significantly during the one-revolution transfer time, preventing GPOPS-II from achieving a converged SC2C transfer. In our experience, we were able to obtain fully converged PMC2C transfers within the domain presented in Sec. V.E.

Because of the very nature of a PMC2C transfer, the number of revolutions N is discrete and unknown a priori. Each orbital revolution adds a discrete time increase δt and a discrete radius change

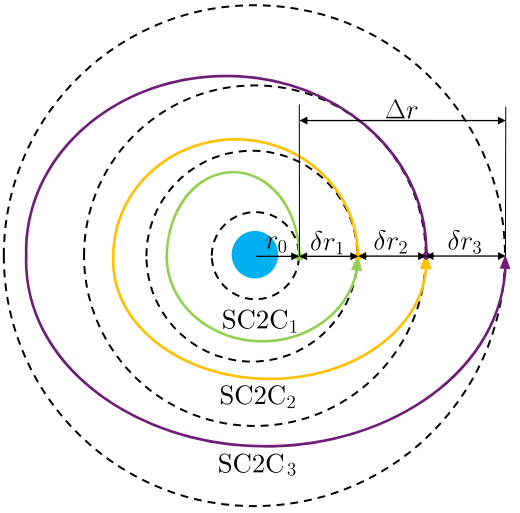

Fig. 3 Schematic of the patching procedure.

δr to the total transfer (see Fig. 3). The final transfer time and radius change are therefore an aggregation of all the individual SC2C transfers (i.e., $\Delta t = \sum_{j=1}^{N} \delta t_j$ and $\Delta r = \sum_{j=1}^{N} \delta r_j$). Our approach to compute a PMC2C transfer is to keep patching SC2C transfers until the desired value for Δr or Δt is reached. Then, the number of revolutions becomes an output of the process.

A. Example Transfer

Figure 4a shows an example PMC2C transfer, where a sail with $a_0 = 0.1$ mm/s^2 is used to execute a transfer of 0.25 years around Earth starting from GEO altitude (i.e., $r_0 = 42,164$ km) and at the autumnal equinox. An inclination of 90 deg and a RAAN of 180 deg are selected to place the orbital plane parallel to the (y_e, z_e) plane and perpendicular to the initial sun–planet direction $\widehat{\boldsymbol{S}}(0)$. Figure 4b shows a zoomed-in view of the region along the $-z_e$ axis where the patching occurs, where darker colors indicate an increasing number of revolutions. In this example, the sail completed $N = 84$ orbital revolutions (i.e., 84 individual SC2C optimizations) before reaching the target transfer time of 0.25 years. The transfer took 9 s to compute in one thread of an `Apple M1 Pro` processor, achieving a final radius change of 3895 km (i.e., $\Delta\rho = 0.092$).

Figure 5 gathers the evolutions of the aspect angle β (Fig. 5a), the scaled radius change $\Delta\rho$ (Fig. 5b), and the osculating eccentricity (Fig. 5c) of the transfer shown in Fig. 4. Let us start the discussion with Fig. 5a. The aspect angle increases linearly from 0 to 90 deg: the orbital plane is perpendicular to the initial sun–planet direction $\widehat{\boldsymbol{S}}(0)$, yielding an initial aspect angle of $\beta(0) = 0$ deg; one-quarter of a year later, the sun–planet direction has moved 90 deg counterclockwise in the ecliptic plane (see how $\widehat{\boldsymbol{S}}$ changes in Fig. 4a), matching the y_e axis, and thus yielding a final aspect angle of $\beta(0.25) = 90$ deg. The scaled radius change in Fig. 5b increases rapidly at first, to flatten out at the end of the transfer: the smaller aspect angles at the beginning of the transfer ensure high SC2C performances in the patched sequence, whereas the larger values at the end of the transfer cause SC2C performance to drop (see Sec. III.B), leading to a slower increase for $\Delta\rho$. The effect can also be appreciated in Fig. 4b, where the curves clump together at the end of the transfer. The nature of the PMC2C transfer is explicitly shown in the eccentricity evolution in Fig. 5c. Note how the eccentricity is brought to zero at every orbital revolution, indicating that the PMC2C transfer is indeed a patched sequence of SC2C transfers. If the eccentricity were allowed to grow throughout the transfer, a more optimal result could be obtained. Initial investigations using collocation techniques to optimize multirevolution circular-to-circular transfers suggest that, for some geometries, it is better to let the eccentricity grow at the beginning of the transfer in order to later bring it down to zero, indicating that the PMC2C transfers are indeed suboptimal. Future work will assess the suboptimality of

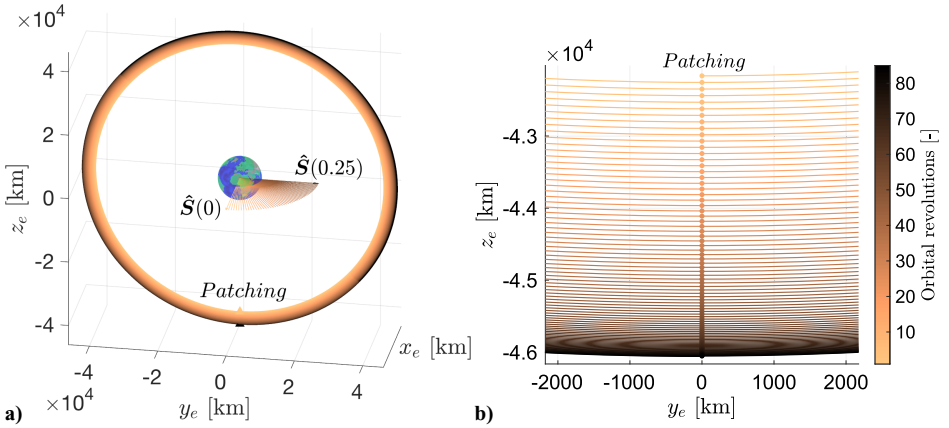

Fig. 4 Example 84-revolution PMC2C transfer around Earth at GEO altitudes with the orbital plane placed perpendicular to the ecliptic plane: a) general three-dimensional view in ecliptic frame, and b) zoomed-in view of the region where the patching occurs.

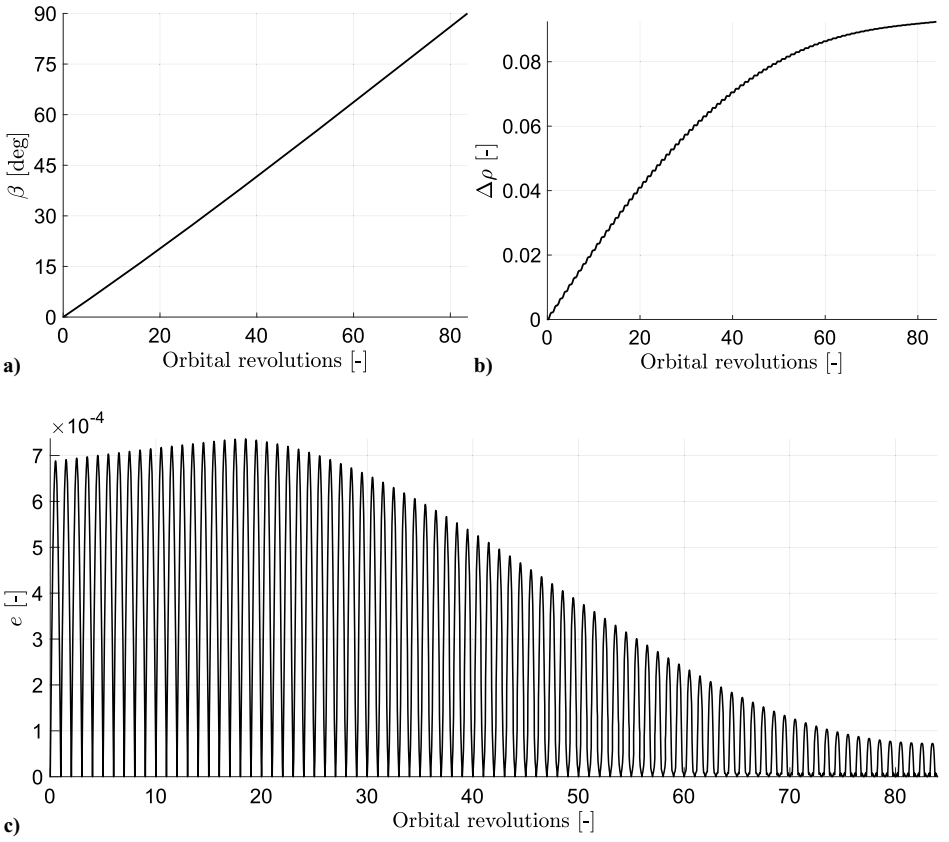

Fig. 5 Example 84-revolution PMC2C transfer around Earth. Evolution as a function of the orbital revolutions of a) the aspect angle β, b) the scaled radius increase $\Delta\rho$, and c) the osculating eccentricity e.

the PMC2C transfers by comparing against optimal multirevolution circular-to-circular transfers.

B. Aspect-Angle Yearly Evolution

As shown in Figs. 4a and 5a, due to the large timescales of a PMC2C transfer (i.e., fractions of a year), we have to relax the fixed-sun assumption used in Sec. III. If the sun is no longer considered fixed in frame I, the sun–planet direction $\hat{\boldsymbol{S}}$ is free to move in the ecliptic plane, yielding a time-varying aspect angle. Because the performance of the PMC2C transfer largely depends on the aspect angle (see Fig. 5b), this section analyzes the yearly evolution of the aspect angle and identifies the best and worst epochs during the year to start a PMC2C transfer.

Figure 6a shows a schematic of the geometry used to compute the yearly evolution of the aspect angle. The schematic depicts the ecliptic reference frame, the ecliptic plane, the orbital plane, and the sun–planet direction at four equally spaced epochs during the year. Figure 6b shows the yearly evolution of the aspect angle for various orbital inclinations, where darker colors indicate larger inclinations. For reference, the light green curve represents the inclination of the GEO orbit. All orbits have an ecliptic RAAN of 0 deg and, at the initial time, the sun–planet direction matches the x axis. When generating the figure, we assumed circular motion of the planet around the star; and in line with the dynamics in Sec. II, the orbits are fixed in inertial space.

Recall that the aspect angle β is defined as the angle between the moving sun–planet direction $\hat{\boldsymbol{S}}$ and the inertial orbit's angular momentum vector $\hat{\boldsymbol{h}}$. According to this definition, $\beta(t) \in [0, \pi]$ for a full year (see the continuous lines in Fig. 6b). As we shall see in Sec. V, we are interested in the function composition $\chi[\beta(t)]$.

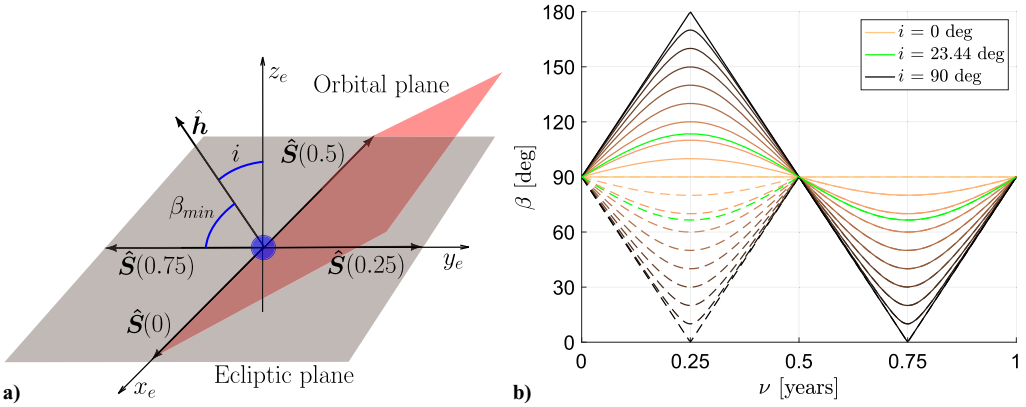

Fig. 6 Representations of a) orbit geometry in the ecliptic reference frame, showing the time-dependent sun–planet direction at four equally spaced epochs during the year; and b) yearly evolution of the aspect angle for 10 deg steps in the inclination (the light green curve represents the inclination of the GEO orbit). The dashed lines represent the aspect angle when reduced to the first quadrant.

Because χ is symmetric with respect to $\pi/2$ (see Sec. III.B), we can simplify and reduce the values for β greater than $\pi/2$ to the first quadrant so that $\beta(t) \in [0, \pi/2]$ (i.e., for those epochs for which $\beta \in (\pi/2, \pi]$, we compute $\beta' = \pi - \beta$ and then replace $\beta = \beta'$). The dashed lines in Fig. 6b represent the case where the aspect angle is reduced to the first quadrant. Hereinafter, we focus the discussion on these curves in the first quadrant.

The aspect angle varies periodically, reaching two minima and two maxima during the year. The maxima are always at $\beta = 90$ deg, and occur when the sun–planet direction matches the line of nodes of the orbit, or, in other words, when the sun–planet direction is contained in the orbital plane (see Fig. 6a at 0 and 0.5 years, respectively). The minima occur exactly one-quarter of a year after the maxima, when the sun–planet direction is perpendicular to the line of nodes of the orbit (see Fig. 6a at 0.25 and 0.75 years, respectively). Due to the geometry of the problem, the value of the minima varies with the inclination of the orbit as $\beta_{\text{min}} = \pi/2 - i$ (see Fig. 6a). One can readily see in Fig. 6b that the evolution of the aspect angle for $i = 90$ deg is the only curve that reaches $\beta = 0$ deg (i.e., the sun–planet direction becomes perpendicular to the orbital plane). As the inclination decreases, the minimum aspect angle increases until, for $i = 0$ deg, the evolution of the aspect angle is a horizontal line at $\beta = 90$ deg (i.e., the orbital plane matches the ecliptic plane). Changing the initial RAAN produces a time shift in the curves of Fig. 6b without changing their shape. Indeed, changing the RAAN is equivalent to changing the initial epoch because it changes the relative geometry between the line of nodes of the orbit and the sun–planet direction.

After close inspection of Fig. 6b, the next two key points arise: 1) to identify the best epoch to start a PMC2C transfer of duration Δt, and 2) to find the inclination that yields the best transfer performance. To address the first point, recall from Fig. 2a that the maximum SC2C performance is achieved for $\beta = 0$ deg. To keep performance close to the maximum during the PMC2C transfer, the transfer timespan Δt must be centered around the minima of the curves in Fig. 6b. Hence, the answer to the first point is as follows: the best epoch t_b to start a PMC2C transfer of Δt is $t_b = t_{\text{min}} - \Delta t/2$, where t_{min} is the epoch at which the minimum aspect angle occurs [i.e., in Fig. 6b, at $\nu = 0.25$ and 0.75 years ($i = 0$ deg excluded)]. Following a similar reasoning, the worst epoch t_w to start a transfer is $t_w = t_{\text{max}} - \Delta t/2$, where t_{max} is the epoch at which the maximum aspect angle occurs [i.e., in Fig. 6b, at $\nu = 0$ and 0.5 years ($i = 0$ deg excluded)]. If the transfer begins at t_b, the achieved change in orbital radius Δr will be greater than if the transfer begins at t_w (i.e., $\Delta r_b > \Delta r_w$). Starting the transfer at any epoch in between t_w and t_b will yield $\Delta r \in [\Delta r_w, \Delta r_b]$.

To address the second point, it suffices to inspect Fig. 6b. The inclination that will yield the largest Δr for a given Δt is 90 deg because the evolution of the aspect angle for $i = 90$ deg is the only one that reaches $\beta = 0$ deg. In contrast, the smallest Δr will occur for $i = 0$ deg because the aspect angle is always 90 deg in that case.

V. Patched Method

The purpose of the patched method is to have a set of formulas that links the radius change Δr with the transfer time Δt of a PMC2C transfer. More precisely, the patched method exploits the characteristics of the SC2C performance η (see Sec. III.B) to provide estimates of the total transfer time Δt and total radius change Δr of a PMC2C transfer without the need to numerically compute the PMC2C transfer itself. Moreover, the set of formulas of the patched method can relate Δr with Δt for any given orbit geometry and initial time. That way, the patched method enables the fast evaluation of many different PMC2C transfers during early mission design.

To derive the sought-for set of formulas, we start with the following differential equation in scaled units that relates a small orbital radius change with a small transfer time:

$$\mathrm{d}\rho = \frac{\mathrm{d}\rho}{\mathrm{d}\tau}\mathrm{d}\tau \tag{6}$$

Because the scaled time τ roughly represents time in orbital revolutions, the time derivative $\mathrm{d}\rho/\mathrm{d}\tau$ can be interpreted as the "change in radius per orbital revolution". Note that, for the particular case of a PMC2C transfer, the change in radius per orbital revolution is, by definition, the performance η of each SC2C transfer in the patched sequence. Hence, using Eq. (5), we can approximate the time derivative as

$$\frac{\mathrm{d}\rho}{\mathrm{d}\tau} \asymp \eta = \eta_r\, \chi \tag{7}$$

Although η is not an instantaneous rate of change, it successfully captures the secular variation of the scaled radius with the scaled time, making Eq. (7) a fair approximation (see validation in Sec. VI). In Sec. III.B, we concluded that, for a fixed sail design, η_r varies with the orbital radius. During a lengthy PMC2C transfer, the orbital radius can change significantly. To capture that effect in the patched method, we further expand η_r as

$$\eta_r = \eta_{r_0}\, \rho^{1+s} \tag{8}$$

where η_{r_0} is the reference performance at the initial conditions of the PMC2C transfer, and s is a coefficient that dictates how performance varies with orbital radius. Combining Eqs. (6–8), we obtain the differential equation that governs the patched method:

$$\mathrm{d}\rho = \eta_{r_0}\, \rho^{1+s} \chi\, \mathrm{d}\tau \tag{9}$$

At this stage, it is convenient to perform a change of variable from scaled time τ to time in years ν. The relationship between both times is $T_0\tau = P\nu$, where P is the orbital period of the planet. Integrating Eq. (9) and applying the change of variable yields

$$\int_1^{1+\Delta\rho} \frac{\mathrm{d}\rho}{\rho^{1+s}} = \eta_{r_0}\frac{P}{T_0}\int_{\nu_0}^{\nu_0+\Delta\nu} \chi\,\mathrm{d}\nu \tag{10}$$

where ν_0 is the initial epoch and $\Delta\nu$ the transfer time in years. To ease readability, Eq. (10) can be condensed to

$$\Lambda = D\Delta\Gamma \tag{11}$$

where Λ captures the left-hand-side integral and is the altitude correction function, $D = \eta_{r_0}P/T_0$ is referred to as the transformation constant, and the right-hand-side integral $\Delta\Gamma$ is coined the leaf function. Below, we analyze each term separately.

A. Altitude Correction Function

The altitude correction function Λ considers the performance variation with altitude in the patched method. It is obtained from analytically evaluating the integral on the left-hand side of Eq. (10):

$$\Lambda = \frac{1}{s}\left[1 - \frac{1}{(\Delta\rho+1)^s}\right] \tag{12}$$

The value for the parameter s is obtained empirically by fitting Eq. (12) to a representative numerically computed PMC2C transfer; see the Appendix for a detailed explanation of the fitting procedure. We then obtain $s = 0.495170003611198$.

Figure 7 shows the evolution of the altitude correction function over the scaled radius change. For increasing values of $\Delta\rho$, the function approaches a horizontal asymptote at $\Lambda = 1/s$ (dashed line). For negative values of $\Delta\rho$, the function approaches a vertical asymptote at $\Delta\rho = -1$ (not shown). Note that neither asymptote can be reached: for large values of $\Delta\rho$, the sail escapes from the planetary system, whereas for $\Delta\rho$ approaching -1, the sail crashes with the surface of the planet. In most practical situations, the scaled radius change is small (e.g., for a transfer from GEO to the graveyard orbit $\Delta\rho = 0.007$) and the effect of the altitude variation on the performance is negligible. Indeed, mathematically from Eq. (12), when $\Delta\rho \ll 1$, $\Lambda \approx \Delta\rho$ (e.g., $\Lambda = 0.007$ for the GEO to graveyard case).

B. Transformation Constant

The transformation constant D can be easily computed from the initial conditions of the transfer and the formulas in Sec. III.B:

$$D = \eta_{r_0}\frac{P}{T_0} = l\,n\Psi^m\frac{P}{T_0} \tag{13}$$

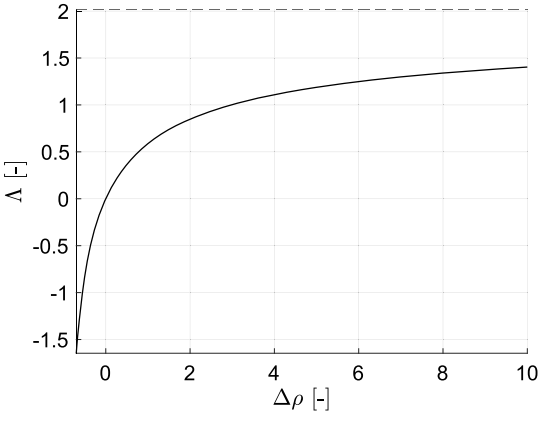

Fig. 7 Altitude correction function.

where $l = \{-1, 1\}$ is the direction parameter. Note that a PMC2C transfer can either increase or decrease the orbital radius. When increasing the orbital radius, the performances of the SC2C transfers in the sequence must always be positive. Conversely, when decreasing the orbital radius, the individual performances must be negative. The direction parameter is introduced to differentiate between the two options: $l = -1$ when decreasing the orbital radius (i.e., $D < 0$), and $l = 1$ when increasing the orbital radius (i.e., $D > 0$).

The term "transformation constant" comes from the fact that it transforms Λ to $\Delta\Gamma$ [see Eq. (11)]. As we saw, in most cases, $\Lambda \approx \Delta\rho$; and, as we shall see, $\Delta\Gamma$ is directly proportional to the transfer time $\Delta\nu$. Hence, in practice, D transforms a target $\Delta\rho$ to the required transfer time $\Delta\nu$.

C. Leaf Function

The leaf function $\Delta\Gamma$ is obtained from numerically evaluating the integral on the right-hand side of Eq. (10). Although the integral can be evaluated by starting from any initial epoch ν_0, we focus on the best and worst possible initial epochs to provide the envelope of the transfer time for a given radius change (or vice versa). In Sec. IV.B, the best and worst possible initial epochs were identified as $\nu_b = \nu_{\min} - \Delta\nu/2$ and $\nu_w = \nu_{\max} - \Delta\nu/2$, respectively. Substituting these epochs into the integration limits yields

$$\Delta\Gamma_k = \int_{\nu_k}^{\nu_k+\Delta\nu} \chi[\beta(\nu)]\,\mathrm{d}\nu \tag{14}$$

where $k = \{b, w\}$ such that ν_k represents both the best and worst initial epochs. Note that $\Delta\Gamma_b \geq \Delta\Gamma_w$ for any given transfer time $\Delta\nu$. Moreover, choosing an initial epoch ν_0 in between ν_w and ν_b will yield $\Delta\Gamma \in [\Delta\Gamma_w, \Delta\Gamma_b]$.

When numerically integrating Eq. (14) for increasing values of $\Delta\nu$, Fig. 8 is obtained. The figure shows the transfer time $\Delta\nu$ in years over $\Delta\Gamma$ for the best and worst initial epochs and for various orbit inclinations, where lighter colors represent smaller inclinations. As in Fig. 6b, we assume circular motion of the planet around the star and that the orbital plane is fixed in inertial space. By inspecting the shapes in Fig. 8, the reader can understand where the term "leaf function" comes from. For each value of the orbit inclination, there are two lines: one linked to the best initial epoch, and one to the worst initial epoch. Note how the best–worst line pairs resemble an array of leaves that become thinner as the orbit inclination decreases. Each leaf is the graphical representation of the bounds of the leaf function $\Delta\Gamma$. Indeed, for an epoch in between the worst and best epochs, we obtain a line inside the corresponding leaf. Figure 8 plays a central role in the patched method, as it allows to easily understand the influence of orbit inclination and initial epoch in the transfer performance.

The characteristics of Fig. 8 can be explained by inspecting Eq. (14) and Fig. 6b. The integral in Eq. (14) is inversely proportional to the area below the curves in Fig. 6b. For $i = 90$ deg, the area below the corresponding curve in Fig. 6b changes significantly, depending on where we start the integration. This is reflected in the wide gap between the best and worst transfer times in Fig. 8. Instead, for $i = 0$ deg, it is not relevant where we start the integration in Fig. 6b, as the corresponding curve is a straight line. This translates into the straight line in Fig. 8 for $i = 0$ deg.

When a transfer time of $\Delta\nu = 0.5$ years is considered, the area below the curves in Fig. 6b is the same, regardless of the initial epoch, causing the best and worst lines in Fig. 8 to intersect. For transfer times greater than 0.5 years (e.g., 0.6 years), the integral in Eq. (14) can be computed as the integral from 0 to 0.5 years plus the integral from 0 to 0.1 years. In other words, the integral in Eq. (14) is periodic with a period of 0.5 years. Hence, for values of $\Delta\nu$ greater than 0.5, Fig. 8 can be expanded by simply stacking the best and worst lines periodically at the intersection point (see Sec. V.D).

Finally, from Fig. 8, it is possible to infer how the inclination influences the transfer performance. For a given value of $\Delta\Gamma$, the transfer time increases as the inclination decreases. The minimum transfer time occurs for the best starting epoch for $i = 90$ deg, and

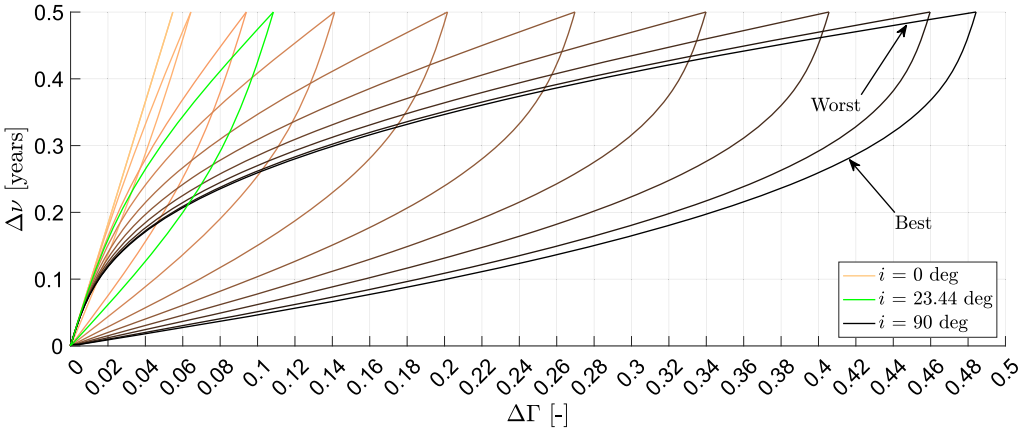

Fig. 8 Best and worst transfer times $\Delta\nu$ in years as a function of the leaf function $\Delta\Gamma$ for 10 deg steps in the inclination. The light green leaf represents the inclination of the GEO orbit.

the maximum transfer time occurs for $i = 0$ deg, when the sun–planet direction lies in the orbital plane at all times.

D. Examples

The set of formulas of the patched method can be used to estimate the performance of PMC2C transfers in two different ways: 1) the "time mode" where, for a given target radius change $\Delta\rho$, we want to obtain the required transfer time $\Delta\nu$; and 2) the "range mode" where, for a given transfer time $\Delta\nu$, we want to obtain the achievable $\Delta\rho$. In addition, the method can be used to estimate these modes for both increasing ("up") and decreasing ("down") the orbital radius.

In the next two subsections, both modes are discussed in more detail and several examples are provided. In both subsections, the following common parameters are used related to the planet (μ, P), the initial epoch (ν_0), the initial circular orbit (r_0, i, Ω), and the sail design (a_0).

1. *Time Mode*

To obtain the transfer time $\Delta\nu$ to reach a given radius change $\Delta\rho$, the following steps need to be taken:

1) Obtain Λ by substituting $\Delta\rho$ in Eq. (12). Note that $\Delta\rho < 0$ when decreasing the orbital radius (down), yielding $\Lambda < 0$.

2) Compute D. First, calculate $\Psi = (a_0 r_0^2)/\mu$ and $T_0 = 2\pi\sqrt{r_0^3/\mu}$. Then, choose the direction parameter l: -1 if down and 1 if up. After that, obtain η_{r_0} from $\eta_{r_0} = l\, n\Psi^m$. Finally, $D = \eta_{r_0} P/T_0$.

3) Evaluate $\Delta\Gamma = \Lambda/D$. Note that, because D and Λ always have the same sign, $\Delta\Gamma > 0$ for both the up and down cases.

4) To end, we need to solve Eq. (14) for $\Delta\nu$. However, $\Delta\nu$ appears in the upper integration bound, which makes Eq. (14) implicit in $\Delta\nu$. We propose a simple bisection strategy to tackle the problem. With the initial geometry of the orbit, one can compute the time evolution of the aspect angle and numerically integrate Eq. (14) up to two arbitrary transfer times $\Delta\nu_1$ and $\Delta\nu_2$ that encompass $\Delta\nu$, where $\Delta\nu_1 < \Delta\nu_2$. Then, given that $\Delta\nu \in [\Delta\nu_1, \Delta\nu_2]$, use a bisection method to iteratively converge to $\Delta\nu$ under a certain tolerance. A more straightforward, although less accurate, option is to use Fig. 8 and obtain $\Delta\nu$ manually from the plot (see the examples in the following).

To put the time mode into practice, we are going to analyze a hypothetical solar-sail debris removal mission around Earth (i.e., $\mu = 3.986004418 \times 10^5$ km^3/s^2, $P = 365.256$ days) using the parameters of the recently launched ACS3 solar sail (i.e., $a_0 = 0.045$ mm/s^2, mass $m = 16$ kg) [6]. The mission consists of two phases: 1) moving a debris object of 130 kg from GEO (i.e., $i = 23.44$ deg, $r_0 = 42{,}164$ km) to the graveyard orbit (i.e., $\Delta r = 300$ km), and 2) transferring from the graveyard orbit back to GEO. Because the exact starting dates (i.e., ν_0 and Ω) are unknown, we are going to obtain the best and worst total mission times in order to gain an understanding of the capabilities of an ACS3-like solar sail for such a mission.

During the first phase of the mission, the characteristic acceleration is reduced to $a_0 = 0.0049$ mm/s^2 due to the extra mass from the debris object. To obtain the transfer time envelope for the first phase, we follow the steps of the time mode workflow: 1) from $\Delta\rho = 0.007$, we obtain $\Lambda = 0.007$; 2) $\Psi = 2.2 \times 10^{-5}$, then $\eta_{r_0} = 4.8 \times 10^{-5}$, which gives $D = 0.0176$; 3) $\Delta\Gamma = 0.4$; and 4) we use Fig. 8 to obtain the best and worst transfer times.

If we enter Fig. 8 at $\Delta\Gamma = 0.4$ and try to intersect the light green curve associated with the GEO inclination, this does not appear to be feasible. The problem is solved by using the periodicity of Eq. (14). Recall from the discussion in Sec. V.C that Eq. (14) is periodic with a period of 0.5 years. Graphically, that means that we can stack an arbitrary number of light green "leaves" to the right of where the one in Fig. 8 ends (i.e., at $\Delta\Gamma_{\max}|_{i=23.44} = 0.108$) until we obtain an intersection for our particular value for $\Delta\Gamma$. Figure 9a illustrates the stacking procedure in this example: four leaves are required before an intersection with the value $\Delta\Gamma = 0.4$ is achieved. The intersection yields the best and worst transfer times for phase one: $\Delta\nu_{b1} = 1.76$ and $\Delta\nu_{w1} = 1.89$ years, respectively.

Equivalently, to avoid having to create Fig. 9a, we can use the modulo operation $\Delta\Gamma \% \Delta\Gamma_{\max}|_{i=23.44}$ to obtain a remainder of $\Delta\Gamma' = 0.076$. The quotient represents the number of extra 0.5 years to be added later: $3 \times 0.5 = 1.5$ years in this case. Figure 9b depicts the modulo operation approach, where we can see that the intersection of $\Delta\Gamma' = 0.076$ with the first leaf is exactly the same as the intersection of $\Delta\Gamma = 0.4$ with the fourth leaf: 0.26 and 0.39 years. The number of full leaves in between is the number of extra 0.5 years to be added to obtain the total transfer times. Hence, we add the extra 1.5 years to obtain the same best and worst transfer times for phase one: $\Delta\nu_{b1} = 1.76$ and $\Delta\nu_{w1} = 1.89$ years, respectively. Following the modulo approach, one does not need to create any additional plots, as the remainder of the modulo operation will always yield an intersection in Fig. 8.

For the second phase, 1) $\Lambda \approx \Delta\rho = -0.007$; 2) the debris is released, returning a_0 to its original value of 0.045 mm/s^2, which yields $D = -0.16$; 3) $\Delta\Gamma = 0.044$; and 4) we enter Fig. 8 to obtain $\Delta\nu_{b2} = 0.14$ and $\Delta\nu_{w2} = 0.28$ years, respectively.

As a final step, we add the transfer times of both phases to obtain the total best and worst transfer times: $\Delta\nu_b = 1.9$ and $\Delta\nu_w = 2.17$ years, respectively. It seems that, for this particular mission, the launch date is not critical because the difference between the worst and best total mission times is only 0.27 years. This hypothetical example shows that with just a calculator and Fig. 8, the mission designer can rapidly assess a large variety of mission scenarios, improving the workflow during early mission design.

2. *Range Mode*

To obtain the achievable radius change $\Delta\rho$ within a given transfer time $\Delta\nu$, the following steps need to be taken:

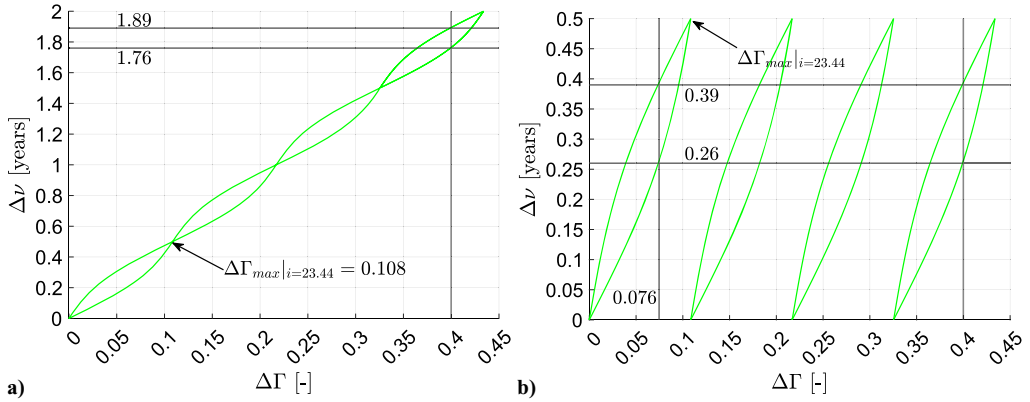

Fig. 9 Example of the stacking procedure using the GEO leaf: a) graphical approach, and b) modulo approach.

1) Compute the aspect-angle curve as in Fig. 6b, associated with the initial orbit, and numerically integrate Eq. (14) for a duration of $\Delta\nu$ years to obtain $\Delta\Gamma$. Again, a more straightforward although less accurate option is to use Fig. 8 to graphically obtain $\Delta\Gamma$.

2) Compute D. First, calculate $\Psi = (a_0 r_0^2)/\mu$ and $T_0 = 2\pi\sqrt{r_0^3/\mu}$. Then, choose the direction parameter l: -1 if down and 1 if up. After that, obtain η_{r_0} from $\eta_{r_0} = l\, n\Psi^m$. Finally, $D = \eta_{r_0} P/T_0$.

3) Evaluate $\Lambda = D\Delta\Gamma$. Note that $\Lambda > 0$ for the up direction and $\Lambda < 0$ for the down direction.

4) Solve for $\Delta\rho$ in Eq. (12). Again, note that $\Delta\rho > 0$ for the up case and $\Delta\rho < 0$ for the down case, as expected.

To put the range mode in practice, consider a Sunjammer-type sail with $a_0 = 0.22$ mm/s^2 [23]. We are going to use the range mode to obtain the change in circular orbit radius after a transfer time of one year, starting from a MEO orbit with $r_0 = 15{,}000$ km and $i = 50$ deg. First, we need to compute $\Delta\Gamma$ for $\Delta\nu = 1$. To do so, we again need to use the periodicity property of Eq. (14). As in the example given for the time mode, we need to sequentially stack the leaf corresponding to $i = 50$ deg until we equal or exceed the given transfer time. In this example, taking into account that one full leaf equals 0.5 years, we need to stack two leaves, yielding $\Delta\Gamma = 2\Delta\Gamma_{\max}|_{i=50} = 0.54$. The rest of the workflow is straightforward: 2) $\Psi = 1.24 \times 10^{-4}$, $\eta_{r_0} = 2.71 \times 10^{-4}$, and thus $D = 0.47$; 3) $\Lambda = 0.47 \times 0.54 = 0.25$; and 4) $\Delta\rho = 0.31$. Finally, in physical units, the sail would be able to change its circular orbit radius by $\Delta r = r_0 \Delta\rho = 4650$ km in one year.

E. Domain of the Method

The patched method produces accurate results within a specific altitude band. We refer to this altitude band as the domain of the patched method. The lower limit of the domain is the surface of the planet, whereas the upper limit can be reached due to two different causes: 1) surpassing the maximum value for Ψ, and 2) reaching an unacceptable change in aspect angle per orbital revolution.

Concerning the first limitation, in Sec. III.B, it was highlighted that Eq. (5) [i.e., one of the core assumptions of the patched method; see Eq. (7)] is valid only if $\Psi < 1 \times 10^{-2}$. When the latter limit is surpassed, the results in Fig. 2 can no longer accurately predict the performance of each SC2C transfer in the PMC2C sequence, causing the predictions of the patched method to diverge from the real values. Using the upper limit $\Psi_{\max} = 1 \times 10^{-2}$ and recalling that $\Psi = a_0/g_0$, we can derive an upper limit for the domain of the patched method. That is, the maximum radius that a PMC2C transfer can reach for the patched method to still provide accurate predictions is

$$r_{\max} = \sqrt{\frac{\mu \Psi_{\max}}{a_0}} \tag{15}$$

The maximum radius is inversely proportional to a_0: the better the sail performs, the narrower the domain of the patched method. Note that the maximum radius refers to the final radius, and not the initial one. It may therefore happen that we analyze a PMC2C transfer that starts below $r_{\max}$ and surpasses $r_{\max}$ midtransfer. In that case, the predictions of the patched method might be inaccurate.

The second limitation comes from the assumption made regarding the aspect angle when computing the performance of the SC2C transfers as defined in Sec. III. As mentioned in Sec. III.A, in general, the period of the SC2C transfer is much smaller than the orbital period of the planet (i.e., $T_0 \ll P$). However, for transfers starting at high altitudes, this might not be the case. As altitude increases, T_0 grows, until at some point, the aspect angle cannot be considered constant during the SC2C transfer and the assumption made in Eq. (7) is no longer valid. It was found, through trial and error, that a reasonable limit for the patched method to hold is an aspect-angle change of 10 deg per revolution. For larger values, GPOPS-II struggled to reach convergence in most cases, implying that a PMC2C trajectory cannot be assembled.

Figure 10 shows the maximum radius as a function of the sail loading σ for all planets in the solar system scaled with the mean equatorial radius of each planet R. Note that, when considering various planets, the characteristic acceleration is no longer the best representation for the performance of a solar sail. The sail loading σ, defined as sailcraft mass over total sail area, is a more convenient parameter [7]. Both parameters are related via $a_0 = 2p/\sigma$, where p is the solar radiation pressure at the planet's mean distance from the sun.

The lines in Fig. 10 extend to the sphere of influence of each planet, represented with empty circular markers. The solid circular markers denote the altitude at which the aspect angle changes 10 deg per revolution, effectively representing the absolute upper bound of the domain. The vertical lines mark three representative sail loadings: current ($\sigma = 0.18$ kg/m^2, $a_0 = 0.05$ mm/s^2 at Earth), near-term ($\sigma = 0.09$ kg/m^2, $a_0 = 0.1$ mm/s^2 at Earth), and future ($\sigma = 0.009$ kg/m^2, $a_0 = 1$ mm/s^2 at Earth) sail technology [24].

The purpose of Fig. 10 is to allow the reader to rapidly obtain the domain of the patched method. For example, using current sail technology around Earth, the domain extends up to the solid circular marker at $r_{\max} \approx 12\,R$ (see how the vertical line representing current technology intersects the black line at the dashed region in Fig. 10). Differently, for a futuristic sail, the upper bound of the domain would reduce to approximately the GEO region (the future-technology line intersects the black line at approximately $r_{\max} \approx 10\,R$).

Finally, it might seem that the lower end of the domain is not the surface of the planet. Indeed, perturbations neglected in this study, such as eclipses and atmospheric drag, are relevant at lower altitudes, suggesting that the patched method cannot be applied for low orbits. However, perturbations do not modify the mathematical formulation of the patched method but instead the performance η of the individual SC2C transfers in the patched sequence. In other words, if one manages to compute η under a more complex dynamical framework (e.g., optical sail model, atmospheric drag, eclipses,

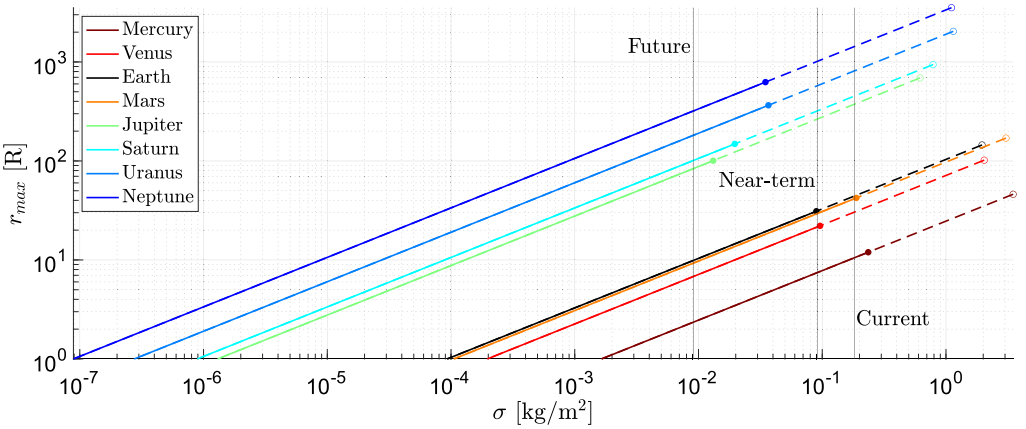

Fig. 10 Domain of the patched method for various planets of the solar system, represented as maximum radius over sail loading. The empty circular markers mark the sphere of influence of each planet, whereas the solid circular markers indicate the point where an aspect-angle variation of 10 deg per revolution is reached.

planetary radiation pressure), the basic differential equation of the patched method [i.e., Eq. (9)] still holds and can be numerically integrated to provide radius change predictions for a given transfer time. Eclipses might be particularly difficult to accommodate. Under long eclipse conditions, it is possible that some of the SC2C transfers in the patched sequence can no longer be computed. A possible fix would be to consider that such failed SC2C transfers do not contribute to the total PMC2C transfer (i.e., the sail is deactivated for such cases). Although relevant, the validation and testing of the mentioned approach is considered outside the scope of this study, whose main objective is to present the equations of the patched method and demonstrate its usage under simple dynamics.

VI. Numerical Validation

The patched method is a semianalytical approach based on the assumption that the time derivative of the radius of the PMC2C transfer can be approximated by the performance of the SC2C transfer [see Eq. (7)]. Moreover, to account for the change in performance with the change in radius, we fit the model to one particular PMC2C transfer (see Sec. V.A), which does not necessarily mean the patched method will perform well for other PMC2C transfers. In this section, we test the correctness and accuracy of the patched method against a range of test cases, proving the validity of the latter assumptions. To do so, we compare the performance estimates obtained using the patched method against the performance obtained directly from PMC2C transfers computed numerically (e.g., PMC2C transfer presented in Sec. IV; see Fig. 4).

A sail with $a_0 = 0.1$ mm/s^2 is used to execute various transfers of 0.25 years around Earth starting at the autumnal equinox. Two cases with different initial altitudes are considered: 1) an LEO case with $r_0 = 7178$ km, and 2) a GEO case with $r_0 = 42,164$ km. In both cases, several inclinations (i.e., 0, 50, and 90 deg) and right ascension of the ascending nodes (i.e., 0 and 90 deg) are taken into account to cover a wide range of orbital geometries. Moreover, both test cases fall within the domain of the method, as established in Sec. V.E.

Figure 11 shows the transfer time $\Delta\nu$ in years as a function of the scaled radius change $\Delta\rho$ for both the LEO (Fig. 11a) and GEO (Fig. 11b) cases, where lighter colors indicate smaller orbit inclinations. There are two lines of the same color per inclination, one for each RAAN, where the "worst" and "best" lines occur for RAANs 0 and 90 deg, respectively. The solid lines correspond to the predictions of the patched method; the circular markers denote the values extracted from the numerical transfers. Note that each marker represents the aggregated discrete radius change obtained after each SC2C in the PMC2C sequence. Due to the smaller effect of the sail on the trajectory in LEO, we can see in Fig. 11a denser population of markers than in Fig. 11b, indicating that more revolutions are required to obtain the same $\Delta\rho$ in LEO than in GEO. In addition, note that in Fig. 11b there is one marker approximately every day.

One can see in Fig. 11 how well the markers follow the solid lines. For a quantitative comparison, Table 1 gathers the absolute and relative error root mean square (RMS) for both test cases, where the error is the difference between the radius change predicted by the patched method and the radius change obtained from the numerical transfers. In addition, Table 2 shows the total runtime comparison between both approaches (i.e., total time it took to compute all cases), where the computation was performed in one thread of an `Apple M1 Pro` processor. The relative error for all geometries considered is smaller than 3 and 2% for the LEO and GEO cases, respectively. The patched method is 7800 and 900 times faster than

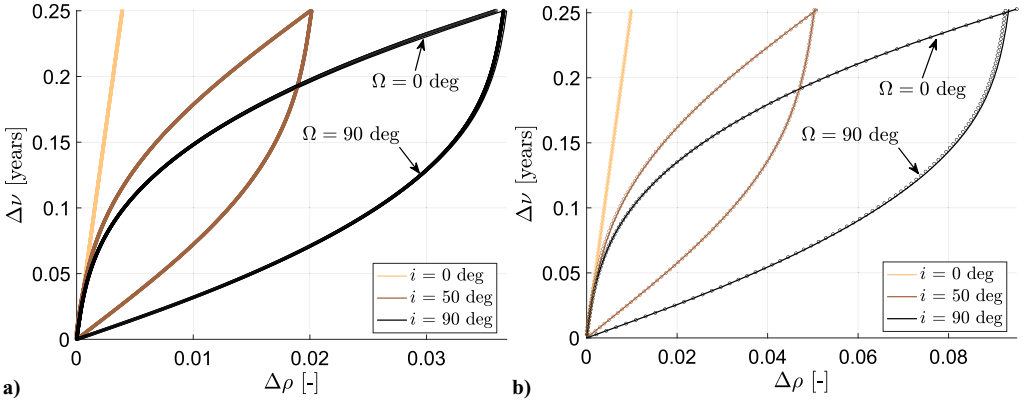

Fig. 11 Transfer time as a function of the scaled radius change for the a) LEO and b) GEO cases. The solid lines correspond to the predictions of the patched method; and the circular markers represent the values obtained from the numerical transfers.

Table 1 Absolute and relative errors

	RMS, km	RMS, %
LEO	1.2	2.6
GEO	7.9	1.7

Table 2 Total runtime comparison

	Method, s	Numerical, s
LEO	0.1	780
GEO	0.1	90

the numerical computation for the LEO and GEO cases, respectively. The small RMS indicates that the patched method accurately represents the PMC2C transfers in these examples, while saving significant computational resources. We believe that the user can expect error levels of the same order of magnitude for any PMC2C transfer that lies in the domain of the patched method. Therefore, within its domain, the patched method can reliably and swiftly predict the transfer time and range of the PMC2C transfers, effectively removing the need to numerically compute them.

VII. Conclusions

This work revealed the basics of how to sail around planets by exploring coplanar patched multirevolution circular-to-circular (PMC2C) transfers. PMC2C transfers are a patched sequence of optimal single-revolution circular-to-circular (SC2C) transfers; the total radius change Δr and total transfer time Δt are obtained as the summation of the individual optimal increments. The PMC2C transfers are not globally optimal, but they might be used as a suitable initial guess for the optimization of coplanar multirevolution circular-to-circular solar-sail transfers, as they effectively connect two arbitrarily separated coplanar circular orbits. Although the computation of a single PMC2C transfer may be achieved in mere minutes, the computational effort quickly increases when generalizing to all possible geometries and sail performances. To overcome this issue, the so-called patched method was proposed. Semianalytical in nature, the patched method estimates the performance (that is, Δr for a given Δt, or vice versa) of PMC2C transfers for any initial condition.

Analyses of the equations governing the patched method reveal the hidden nature of planet-centered solar sailing. The best and worst geometries for a PMC2C transfer occur for an inclination with respect to the ecliptic plane of 90 and 0 deg, respectively. Moreover, the influence of the initial epoch on the transfer performance is remarkable. The best and worst transfer times are identified and visually presented, providing mission designers with a graphical tool to assess the transfer time envelope in a matter of minutes. In general, the best and worst initial epochs occur near to when the sun–planet direction is perpendicular and parallel to the line of nodes of the orbit, respectively. Finally, changing the right ascension of the ascending node of the orbit is equivalent to changing the initial epoch of the transfer, as it changes the relative orientation of the sun–planet direction and the orbit's line of nodes.

The patched method is dimensionless, meaning that it can provide results for any solar-sail design and for solar-sail transfers around any planet orbiting a star. However, it is only valid within a specified altitude band. If the initial altitude of the PMC2C trajectory is too high, the assumptions required to formulate the patched method are violated. In addition, the better the performance of the solar sail, the narrower the altitude band where the model is valid. It was shown that, even for futuristic sail performances, the altitude bands in the solar system remain large enough to render the patched method useful in the far future.

One of the limitations of the patched method is the two-dimensional assumption. The PMC2C transfers are constrained to remain in the initial orbital plane. In reality, the out-of-plane solar-sail acceleration causes an oscillatory motion around the initial orbital plane. Due to the periodicity of the control law, the net inclination error after one single revolution is almost zero. However, for lengthy transfers (that is, more than one year), this error might accumulate, yielding secular errors of the order of 1 deg. Moreover, the patched method cannot provide estimates for missions requiring large plane changes.

When comparing the radius change estimates of the semianalytical patched method against the radius change obtained from the numerically computed PMC2C transfers, it was found that the error introduced by the patched method remained below 3% across all cases considered for a 1000-fold runtime reduction, rendering the patched method an ideal tool for early mission design. It is believed that tools like the patched method will ease the design of solar-sail missions around Earth, paving the way for planet-centered solar sailing.

Appendix: Fitting

The larger the radius change in a PMC2C transfer, the larger the effect of the altitude on the performance of the individual SC2C transfers. We consider a lengthy PMC2C transfer (i.e., $\Delta\rho = 9.4$ and $\Delta\nu = 1.04$) to capture this effect in s. The initial parameters of the fitted transfer are: $a_0 = 0.095$ mm/s^3, $h_0 = 0$ km, $i = 90$ deg, RAAN = 90 deg, $D = 1.33$, and $\Psi = 9.7 \times 10^{-5}$. Note that the initial altitude was set to an unrealistic value of 0 km to maximize $\Delta\rho$.

The parameter s in Eq. (12) is obtained by fitting the numerically computed transfer via nonlinear least squares. Figure A1 gathers the results of the fitting process. The obtained value is $s = 0.495170003611198$, and the residual RMS is 4.95×10^{-3}. Figure A1a shows the fitted altitude correction function (solid line) together with the discrete values (red circular markers) of the numerical PMC2C transfer (i.e., sample values are obtained at the end of each SC2C transfer in the sequence). The low value of the RMS of the altitude correction function implies that the chosen model is appropriate to represent the numerical data.

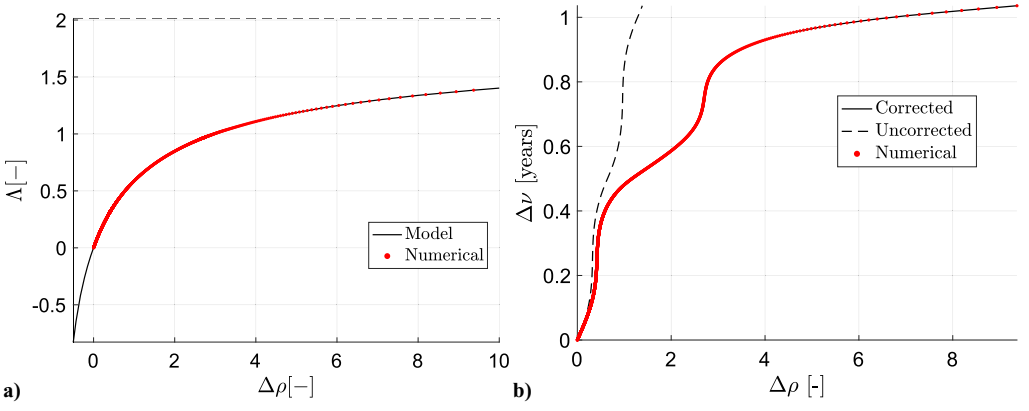

Fig. A1 Results of the fitting: a) fitted altitude correction function, and b) comparison between corrected and uncorrected predictions.

Figure A1b shows $\Delta\nu$ as a function of $\Delta\rho$ for the computed transfer (red circular markers) together with the predictions of the patched method using $s = 0$ (i.e., no altitude correction; dashed line) and the fitted value (i.e., altitude correction; solid line). The large difference between the predicted values highlights the importance of applying the altitude correction, especially when the value of $\Delta\rho$ is large.

Although there is no mathematical proof that guarantees that the obtained value for s is valid for all transfers, we found that the value computed in this Appendix accurately represents a wide range of different test transfers. We fitted s to transfers with increasing values of $\Delta\rho$ and various geometries, and we found s to approach asymptotically a constant value, implying that we just needed to consider a transfer with a sufficiently large $\Delta\rho$ to obtain the correct value for s.

Acknowledgment

This work was funded by a Vidi Grant of the Dutch Research Council (NWO), project number 19690: SWEEP—Space-Waste Elimination around Earth by Photon Propulsion.

References

[1] Tsuda, Y., Mori, O., Funase, R., Sawada, H., Yamamoto, T., Saiki, T., Endo, T., Yonekura, K., Hoshino, H., and Kawaguchi, J., "Achievement of IKAROS—Japanese Deep Space Solar Sail Demonstration Mission," *Acta Astronautica*, Vol. 82, No. 2, 2013, pp. 183–188. https://doi.org/10.1016/j.actaastro.2012.03.032

[2] Johnson, L., Whorton, M., Heaton, A., Pinson, R., Laue, G., and Adams, C., "NanoSail-D: A Solar Sail Demonstration Mission," *Acta Astronautica*, Vol. 68, No. 5, 2011, pp. 571–575. https://doi.org/10.1016/j.actaastro.2010.02.008

[3] Betts, B., Nye, B., Vaughn, J., Greeson, E., Chute, R., Spencer, D. A., Ridenoure, R. W., Munakata, R., Wong, S. D., and Diaz, A., "Lightsail 1 Mission Results and Public Outreach Strategies," *4th International Symposium on Solar Sailing*, 2017, pp. 17–20, https://www.researchgate.net/publication/312331303_International_Symposium_on_Solar_Sailing_2017_Welcome_to_my_session_and_my_presentation.

[4] Spencer, D. A., Betts, B., Bellardo, J. M., Diaz, A., Plante, B., and Mansell, J. R., "The LightSail 2 Solar Sailing Technology Demonstration," *Advances in Space Research*, Vol. 67, No. 9, 2021, pp. 2878–2889. https://doi.org/10.1016/j.asr.2020.06.029

[5] McNutt, L., Johnson, L., Kahn, P., Castillo-Rogez, J., and Frick, A., "Near-Earth Asteroid (NEA) Scout," *AIAA Space, Conference and Exposition*, AIAA Paper 2014-4435, 2014. https://doi.org/10.2514/6.2014-4435

[6] Wilkie, W. K., "Overview of the NASA Advanced Composite Solar Sail System (ACS3) Technology Demonstration Project," *AIAA Scitech 2021 Forum*, AIAA Paper 2021-1260, 2021. https://doi.org/10.2514/6.2021-1260

[7] McInnes, C. R., *Solar Sailing: Technology, Dynamics and Mission Applications*, Springer Science & Business Media, New York, 2004, pp. 151–164.

[8] Coverstone, V. L., and Prussing, J. E., "Technique for Escape from Geosynchronous Transfer Orbit Using a Solar Sail," *Journal of Guidance, Control, and Dynamics*, Vol. 26, No. 4, 2003, pp. 628–634. https://doi.org/10.2514/2.5091

[9] Mengali, G., and Quarta, A. A., "Earth Escape by Ideal Sail and Solar-Photon Thrustor Spacecraft," *Journal of Guidance, Control, and Dynamics*, Vol. 27, No. 6, 2004, pp. 1105–1108. https://doi.org/10.2514/1.10637

[10] Macdonald, M., and McInnes, C. R., "Realistic Earth Escape Strategies for Solar Sailing," *Journal of Guidance, Control, and Dynamics*, Vol. 28, No. 2, 2005, pp. 315–323. https://doi.org/10.2514/1.5165

[11] Mengali, G., and Quarta, A. A., "Near-Optimal Solar-Sail Orbit-Raising from Low Earth Orbit," *Journal of Spacecraft and Rockets*, Vol. 42, No. 5, 2005, pp. 954–958. https://doi.org/10.2514/1.14184

[12] Stolbunov, V., Ceriotti, M., Colombo, C., and McInnes, C. R., "Optimal Law for Inclination Change in an Atmosphere Through Solar Sailing," *Journal of Guidance, Control, and Dynamics*, Vol. 36, No. 5, 2013, pp. 1310–1323. https://doi.org/10.2514/1.59931

[13] Barles, A., Ceriotti, M., Ciampa, F., and Felicetti, L., "An Optimal Steering Law for Sailing with Solar and Planetary Radiation Pressure," *Aerospace Science and Technology*, Vol. 118, Nov. 2021, Paper 107051. https://doi.org/10.1016/j.ast.2021.107051

[14] Carzana, L., Visser, P., and Heiligers, J., "Locally Optimal Control Laws for Earth-Bound Solar Sailing with Atmospheric Drag," *Aerospace Science and Technology*, Vol. 127, Aug. 2022, Paper 107666. https://doi.org/10.1016/j.ast.2022.107666

[15] Fitzgerald, R. M., "Characterizing Minimum-Time Solar Sail Geostationary Orbit Transfers Using Pseudospectral Optimal Control," *Journal of Spacecraft and Rockets*, Vol. 58, No. 4, 2021, pp. 997–1009. https://doi.org/10.2514/1.A34950

[16] Kelly, P., and Bevilacqua, R., "Geostationary Debris Mitigation Using Minimum Time Solar Sail Trajectories with Eclipse Constraints," *Optimal Control Applications and Methods*, Vol. 42, No. 1, 2020, pp. 279–304. https://doi.org/10.1002/oca.2676

[17] Bianchi, C., Niccolai, L., Mengali, G., and Ceriotti, M., "Preliminary Design of a Space Debris Removal Mission in LEO Using a Solar Sail," *Advances in Space Research*, Vol. 73, No. 8, 2024, pp. 4254–4268. https://doi.org/10.1016/j.asr.2024.01.024

[18] Oguri, K., Lantoine, G., Petropoulos, A. E., and McMahon, J. W., "Solar Sailing Q-Law for Planetocentric, Many-Revolution Sail Orbit Transfers," *Journal of Guidance, Control, and Dynamics*, Vol. 46, No. 10, 2023, pp. 2005–2014. https://doi.org/10.2514/1.G007103

[19] Gámez Losada, F., Visser, P., and Heiligers, J., "Fundamentals of Solar-Sail Transfers Around Planetary Bodies," *29th International Symposium on Space Flight Dynamics*, European Space Operations Centre (ESOC), of the European Space Agency (ESA) and the European Organisation for the Exploitation of Meteorological Satellites (EUMETSAT), 2024.

[20] Patterson, M. A., and Rao, A. V., "GPOPS-II: A MATLAB Software for Solving Multiple-Phase Optimal Control Problems Using hp-Adaptive Gaussian Quadrature Collocation Methods and Sparse Nonlinear Programming," *ACM Transactions on Mathematical Software*, Vol. 41, No. 1, 2014, pp. 1–37. https://doi.org/10.1145/2558904

[21] Biegler, L. T., and Zavala, V. M., "Large-Scale Nonlinear Programming Using IPOPT: An Integrating Framework for Enterprise-Wide Dynamic Optimization," *Computers & Chemical Engineering*, Vol. 33, No. 3, 2009, pp. 575–582. https://doi.org/10.1016/j.compchemeng.2008.08.006

[22] Weinstein, M. J., and Rao, A. V., "A Source Transformation via Operator Overloading Method for the Automatic Differentiation of Mathematical Functions in MATLAB," *ACM Transactions on Mathematical Software*, Vol. 42, No. 2, 2016, pp. 1–44. https://doi.org/10.1145/2699456

[23] Heiligers, J., Diedrich, B., Derbes, W., and McInnes, C., "Sunjammer: Preliminary End-to-End Mission Design," *AIAA/AAS Astrodynamics Specialist Conference*, AIAA Paper 2014-4127, 2014. https://doi.org/10.2514/6.2014-4127

[24] Berthet, M., Schalkwyk, J., Çelik, O., Sengupta, D., Fujino, K., Hein, A. M., Tenorio, L., Cardoso dos Santos, J., Worden, S. P., Mauskopf, P. D., et al., "Space Sails for Achieving Major Space Exploration Goals: Historical Review and Future Outlook," *Progress in Aerospace Sciences*, Vol. 150, Oct. 2024, Paper 101047. https://doi.org/10.1016/j.paerosci.2024.101047

F. Topputo
Associate Editor